Solid State Sciences 132 (2022) 106958

Contents lists available at ScienceDirect

Solid State Sciences

journal homepage: www.elsevier.com/locate/ssscie

Ternary metal oxide filled PEO-based polymer electrolyte for solid-state lithium metal battery: The role of filler particle size

Balasubramaniam Ramkumar [a], Vanchiappan Aravindan [b,**], Harivignesh Ramasamy [a], Kanalli V. Ajeya [c], Je-Gwang Ryu [a], Ho-Young Jung [c,d], Yun-Sung Lee [a,*]

[a] Faculty of Chemical Engineering, Chonnam National University, Gwangju 61186, Republic of Korea
[b] Department of Chemistry, Indian Institute of Science Education and Research (IISER) Tirupati 517507, India
[c] Department of Environment and Energy Engineering, Chonnam National University, Gwangju 61186, Republic of Korea
[d] Center for Energy System, Chonnam National University, Gwangju 61186, Republic of Korea

ARTICLE INFO

Keywords:
Composite polymer electrolytes
Polyethylene oxide
Solid-state battery
Lithium-metal batteries
Ceramic fillers

ABSTRACT

Composite polymer electrolytes with fillers exhibit appealing properties, such as high ionic conductivity, good flexibility, and low cost. However, poor compatibility and electrochemical instability, especially at high current rates, are the disadvantages of these electrolytes. In this study, we report the influence of particle size of Li_2O. SiO_2. TiO_2. P_2O_5 (LSTP) on polyethylene oxide (PEO)-matrix towards the fabrication of Li-metal batteries with a $LiFePO_4$ cathode. Compared to micron-sized particles, the high surface area of the nanoparticles in the polymer matrix is beneficial for improved electrochemical stability at 0.1 mA cm^{-2}. Furthermore, the nanosized particulates facilitate faster ionic conductivity (1.09×10^{-3} S cm^{-1} at 80 °C) and excellent stability at higher voltage >4.5 V. Our results clearly indicate the role of filler morphology in enhancing the ionic conductivity and stability. Finally, the full cell made of metallic Li anode and $LiFePO_4$ cathode displays a capacity of 110 mAh g^{-1} (after 100 cycles under 1C at 60 °C) with a reasonable cycle life using such a nanocomposite solid polymer electrolyte.

1. Introduction

The world is facing considerable environmental challenges due to conventional energy sources like fossil fuels and greenhouse gases. To address these issues, rechargeable energy storage systems play an important role as they could store energy from sustainable energy sources like wind, solar, etc., and help to overcome its intermittent nature. These energy storage systems have become ubiquitous over the years. Especially Li-ion batteries (LIB) with good storage capacity and cycle life and has the major share in a wide array of applications [1–3]. LIBs are used so far have Lithium layered oxide as a cathode and graphite anode. The cathode chemistry has evolved from $LiCoO_2$ to high Nickel rich NMC(Ni > 0.8) base structures to meet the demand of the consumers. Despite its huge improvement in the cathode, the anode remains graphite with a theoretical capacity of 372 mAh g^{-1}. Also, graphite suffers from many issues like Li-platting at low temperatures and poor solid electrolyte interphase (SEI) layer formation, which further impedes its performance. Hence, finding an alternating anode with high theoretical capacity and better electrolyte compatibility is preferred for practical applications. In this aspect, Li-metal anodes (3860 mAh g^{-1}) have attracted immense attention in the energy storage field because of their high energy density, lightweight, and shape versatility which has 10 times higher capacity than graphite [4,5]. Initially, the formation of Li-dendrites during cycling was an obstacle to the development of Li-metal anode batteries. This led to the change from "Li-metal" to "Li-ion" batteries, followed by commercialization. Currently, the development of liquid-free electrolytes, *that is*, solid electrolyte systems, has received significant attention. These inorganic solid electrolytes ensure thermal stability but have their own drawbacks like dendrite formation, lower charge transfer kinetics, and poor compatibility with electrode materials [4]. One of the primary focuses of the scientific community is to improve the solid electrolyte/Li-metal interface issues that hinder the commercialization of all-solid-state Li-ion batteries (ASSLIBs). This also creates the possibility to develop new kinds of electrolytes that is more versatile and have good compatibility with electrodes [6,7]. Currently, many research groups are

* Corresponding authors.
** Corresponding authors.
E-mail addresses: aravindan@iisertirupati.ac.in (V. Aravindan), leeys@chonnam.ac.kr (Y.-S. Lee).

https://doi.org/10.1016/j.solidstatesciences.2022.106958
Received 12 April 2022; Received in revised form 24 June 2022; Accepted 25 June 2022
Available online 29 June 2022

involved in addressing interfacial dynamics using suitable solid electrolytes to develop the next-generation Li-metal batteries.

In general, composite solid polymer electrolytes are promising candidates because of their shape versatility, excellent mechanical and electrochemical stability, and leak proofing ability [8]. Among the various polymer electrolytes reported, polyethylene oxide (PEO) is considered to be the most promising matrix owing to its ability to solvate a wide range of Li-salts through the interaction of its ether oxygens with cations. These electrolytes have been extensively investigated as promising candidates for preparing thinner, lighter, and safer batteries [9]. However, their widespread use has been hindered by their intrinsic problems, such as inferior ionic conductivity at 25 °C, poor thermal and chemical stability, and limited potential window [10–12]. Therefore, it is imperative to develop a safe electrolyte with high ionic conductivity, good electrochemical and mechanical properties, and thermal stability. This electrolyte can be used as the Li-ion conducting electrolyte in ASSLMB designs in a free-standing form without modifying the present battery fabrication processes. In polymer-based electrolytes, polymers play a vital role in hosting the Li ions and their ionic transport behavior, such as diffusion in liquid. At the glass-transition temperature, the polymer chains freely move, and the Li ions move in the space between the free volumes of the polymer host [13]. Generally, semi-crystalline PEO is employed as a polymer electrolyte in which the amorphous phase enables the fast transfer of Li ions, while the crystalline units are responsible for mechanical stability. However, the crystalline nature of the PEO disrupts the ionic transport because chain motion is restricted at 25 °C [14,15]. Therefore, ionic transport can be efficiently improved by reducing the crystallinity or expanding the amorphous domains.

Inorganic ceramic solid electrolytes have attracted considerable attention because of their good thermal and electrochemical stability and ionic conductivity at 25 °C. However, their flexibility and shape versatility are problems that need to be addressed [16]. Meanwhile, ceramic electrolytes exhibit superior ionic conductivity than in the case of polymer electrolytes and are highly competitive with conventional liquid electrolytes. Their Li-ion transference number is close to 1, which is essential to achieving high power density. Perovskite, garnet, and NASICON-type structures have been extensively studied as solid electrolytes for LIBs [17–19]. However, the fabrication of ceramic electrolytes is complex, and there is a large energy barrier for ion transfer across the electrode/electrolyte interfaces [20]. Further, the formation of Li dendrite during electrochemical cycling and the brittle nature of the ceramic electrolytes restrict their use in LIBs [20]. Hence, designing flexible CPEs comprising the ceramic filler in a polymer matrix could mitigate the individual drawbacks of ceramic and polymer electrolytes. The resulting composite electrolyte has high ionic conductivity without compromising the mechanical flexibility, thermal stability, and electrochemical compatibility with the electrodes [21–23].

Studies have reported various strategies for improving the electrochemical properties of PEO-composite electrolytes, such as co-polymerization, cross-linking and interpenetration, blending, and inclusion of fillers [11,14,15,19]. To satisfy the demand for high energy and high power density ASSLMB, the electrolyte must function at a high current density. Although the CPE exhibits favorable features for building batteries with shape versatility, the poor-rate performance and stability of the ceramic filler in a polymer matrix remain a major obstacle. The low ionic conductivity and poor mechanical stability of CPEs cause weak interaction between the ceramic filler and polymer matrix. We postulated that reducing the particle size of fillers can increase the contact area and enhance the strong interaction between polymer and filler and thereby improve the ionic conductivity of the electrolyte. Herein, we prepared a new PEO-LSTP composite solid polymer electrolyte and investigated its electrochemical behavior using micron and nano-size ceramic fillers. This study provides an insight into the major understanding of the role of particle size in composite electrolytes to attain high ionic conductivity and high-rate capability, especially at elevated temperature conditions (80 °C). Further, the as-prepared nm-LSTP CPEs were employed as a separator-cum-electrolyte in a Li/$LiFePO_4$ configuration and displayed a capacity of 124 mAh g^{-1} at a rate of 1C in the elevated temperature condition (60 °C). The preparation, design, and engineering of the CPEs along with the necessary structural, morphological, thermal, and electrochemical analyses, were conducted to understand the influence of particle size.

2. Experimental section

2.1. Preparation of PEO-LSTP composite electrolyte

The LSTP micro and nanoparticles were obtained from Jeong Kwan. Co. Ltd. and stored in an Argon-filled glovebox. The size of the particles was approximately 1 μm and 300 nm. Before processing, the PEO (Alfa Aesar, M_v = 10,00,000 g/mol) and LiTFSI salt (Wako) were dried at 50 °C and 100 °C for 24 h under a vacuum to remove moisture, if any. Anhydrous acetonitrile was used to prepare the PEO-LiTFSI solution at a molar ratio of 18:1.25 wt% of the nm and μm LSTP particulates were chosen and separately added to the PEO-LiTFSI solution and mixed for 5 h to obtain a homogenous solution. The prepared slurry was then cast on the surface of a Mylar sheet and dried in an Argon-filled glove box. The diameter and thickness of the CPE were 1.6 cm and approximately 96 μm, respectively.

2.2. Electrochemical characterization of the PEO-LSTP composite and solid-state battery

The olivine phase $LiFePO_4$ cathode was prepared by a routine solution casting process. $LiFePO_4$ (MTI corporation), Super-P, CPE, and polyvinylidene fluoride (PVdF) (6:2:1:1 wt%) were ground in a mortar and then mixed with N-methyl pyrrolidone (NMP) solvent. The mixed slurry was cast on an aluminum foil current collector, and the electrode was vacuum dried at 80 °C for 12 h. In the cathode, the $LiFePO_4$ loading was estimated to be ~1.5–2 mg cm^{-2} per electrode. The electrochemical studies were performed using CR2032 coin cells assembled inside an Argon-filled glove box with an H_2O level below 0.01 ppm. The cells consisted of the $LiFePO_4$ cathode and Li-metal as the anode separated by nanosized LSTP-filled CPEs. Prior to the electrochemical studies, the cell was kept at 60 °C for 24 h in the oven to improve interfacial contacts across the electrode/electrolyte interface (scheme provided in Fig. 1 a). For comparison, we assembled a liquid cell using a polypropylene separator with 1 M $LiPF_6$ in a mixture of ethylene carbonate (EC) and dimethyl carbonate (DMC) (1:1, v:v) as the electrolyte. The electrochemical performance of the liquid cell was tested at 25 °C.

2.3. Material characterization

The powder X-ray diffraction (XRD) was performed using Cu Kα radiation (Rint 1000, Rigaku, Japan). The surface area measurement of the LSTP particles was analyzed using a surface area analyzer (BEL, Japan, Belsorp mini II). The stoichiometric ratio of the LSTP particles was calculated using the inductively coupled plasma–optical emission spectrometry (ICP-OES, PerkinElmer OPTIMA 8300). The surface morphology and particle distribution were evaluated using field emission scanning electron microscopy (FE-SEM) (S-4700, Hitachi, Japan) and optical microscopy with atomic force microscopy (AFM) (XE-100), respectively. Thermal studies were performed on the starting materials and CPE samples in an air atmosphere between RT and 700 °C using thermogravimetric analysis (TGA-TA Instrument TGA Q 500), while differential scanning calorimetry (DSC-TA Instrument DSC Q 2000) was employed from RT to 200 °C. Meanwhile, the FT-IR spectra were used to identify the functional groups of the sample between 400 and 4000 cm^{-1} using an FT-near Infrared Spectrometer (Thermo Fisher Scientific Nicolet Continuum IR Microscope). Meanwhile, the surface and interfacial elemental analysis of the electrolytes were studied by using an X-

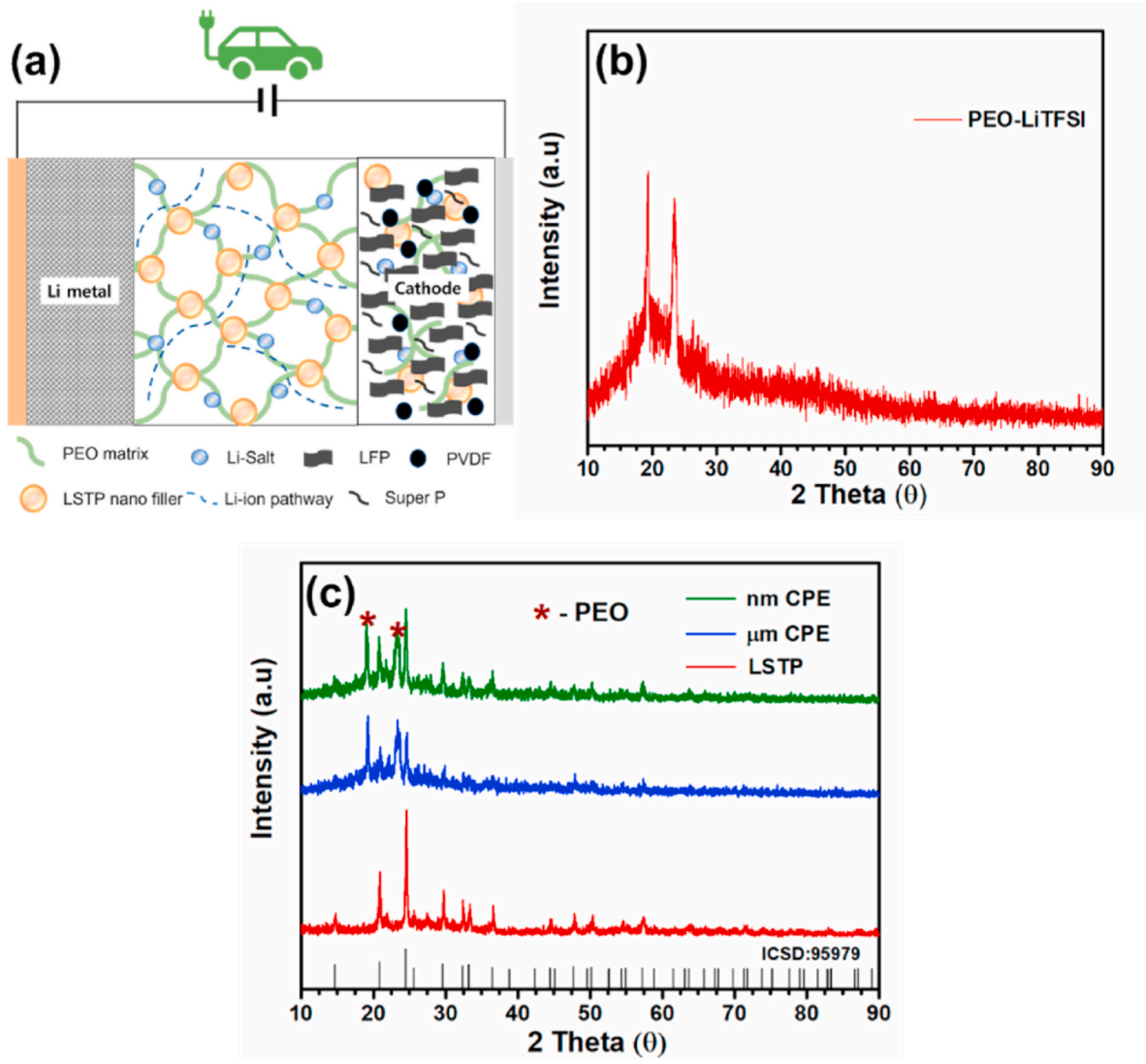

Fig. 1. (a) Schematic of the $LiFePO_4$/nm-LSTP-PEO electrolyte/Li composite solid electrolyte-based composite state battery, XRD pattern of the (b) PEO-LiTFSI electrolyte, and (c) CPEs filled with μm and nm LSTP particles.

ray photoelectron spectrometer (XPS – (ESCA) VG, UK MultiLab2000). The chemical structure analysis of the electrolytes was analyzed using a Nuclear magnetic resonance spectrometer (400 MHz NMR, JEOL, ECZ400R). The two parallel surfaces of the films were attached to a stainless-steel plate to ensure good electrical contact. The ionic conductivity of the cells was measured at a constant voltage (10 mV) using AC impedance analysis (HP 4284A LCR meter), while the transference number and galvanostatic charge-discharge performance were investigated using an electrochemical analyzer (SP-150, Biologic, France). The electrochemical impedance spectra and cyclic voltammetry were analyzed using an electrochemical instrument (VSP, Biologic, France). The charge/discharge and rate capability performance of the nano-CPE in a Li-metal battery with a $LiFePO_4$ cathode, *that is*, an ASSLMB composite solid-state battery, were studied at 60 °C using a III PNE power & supply solution system (PEBC60.1).

3. Results and discussion

3.1. Physical characterization of the composite electrolyte

3.1.1. Analysis of the crystal structure, functional groups, oxidation states

Fig. 1b shows the XRD pattern of the PEO and LiTFSI salt mixture with prominent reflections indicating the characteristic peaks of the respective crystalline domains. The XRD pattern of the PEO-LSTP-based CPEs with different filler sizes is shown in Fig. 1c, along with that of the pure LSTP. The PEO, LSTP, and LiTFSI salt are the main components of the CPEs. The lithium salt would bring low crystallinity in the polymer matrix after it is dissolved in PEO. The strong crystalline peaks corresponding to the PEO are absent in Fig. 1b, indicating the full dissolution of LiTFSI in the polymer matrix. According to the PEO phase/salt phase diagram, the composite mixture preserves a "crystalline gap" that inherently retains the amorphous state at RT [24]. A significant drop in the PEO peak intensity was observed as the ceramic filler was incorporated, which implies that the Li salt and filler could reduce the crystallinity of the PEO, specifically, the peak positions located at $2\theta = 19.2°$ and 23.6° [25,26]. Fig. S1 shows the isotherms of nitrogen adsorption/desorption are applied to study the surface area of the micro and nano-sized LSTP particles. The calculated BET surface area for micro and nanoparticles are 10.811 and 18.647 $m^2\ g^{-1}$, respectively. Table S1 shows the ICP-OES results for the LSTP particles, and the calculated stoichiometric ratio is $Li_{1.06}\ Ti_{1.33}\ Si_{0.18}(PO_4)_3$. The chemical identity, complex formation, and interaction between the various elements of the CPEs were examined using FTIR spectroscopy. The FTIR spectra of the PEO and CPEs filled with nano-, and micron-sized particles were

recorded and are illustrated in Fig. 2. The observed vibrational peak positions and their assigned characteristics are as follows: two peaks appearing at ~1350 and ~1332 cm^{-1} were associated with CH_2 wagging [26], the C–O–C stretching appeared at ~1099 cm^{-1} [27], the two prominent vibrational modes located at ~960 and ~945 cm^{-1} were associated with the CH_2–CH_2 rocking, and C–O–C vibration modes, respectively [27,28], and the peak observed at ~840 cm^{-1} was attributed to the CH_2 wagging mode of the PEO [28,29]. Further, the C–O–C vibration mode had a notable change in width and intensity, which was mainly attributed to the electrostatic interaction between the Li^+ metal ion and ether oxygen in PEO [30]. Fig. 2b depicts that the hydroxyl band (O–H band) of the PEO was positioned at ~3612 cm^{-1} and shifted to ~3462 cm^{-1} due to the bond between the Li^+ ion and host of the polymer backbone [26,31,32]. Fig. 2c shows that the C–H asymmetric bending shifted to ~1456 cm^{-1}. Meanwhile, 1465 cm^{-1} was attributed to the coordination of the oxygen atoms in the PEO and Li^+ ions in the ceramic filler [31]. After the incorporation of the ceramic filler, the vibrational bands broadened, indicating that the nature of the amorphous domains was enhanced. The amorphous regions are responsible for the enhanced ionic mobility of the composite electrolyte [33]. FTIR spectra were obtained to identify the presence of LSTP in the prepared CPEs, as shown in Figs. S2a and S2b. The stretching vibration of the P–O bands in the PO_4 tetrahedral was observed between 1200 and 900 cm^{-1}. The fundamental characteristic peak of the asymmetric stretching of the P–O vibration band was located at ~1120, ~1054, and ~1046 cm^{-1}, which is consistent with the P–O vibration modes of the PO_4^{3-} anions [34,35]. Meanwhile, the crystallinity of the particle influenced the peak position of the nanosized LSTP-based CPEs. The low-intensity peaks located in the range of 800–650 cm^{-1} could be assigned to the Ti–O octahedron [36–38]. The structural distortion in the rhombohedral units was attributed to the Ti^{4+} substituted by Si^{4+} in the spectra [38].

X-ray photoelectron spectroscopy (XPS) is a powerful surface analyzing tool, and it has been extensively used to study battery materials because of its ability to identify, quantify and image the chemical distribution of the elements. Fig. 3 and Figs. S3 and S4 illustrate the typical XPS spectra of C 1s, O 1s, S 2p, F 1s, Si 2p, Ti 2p, and P 2p elements for the CPEs with micro and nano-sized ceramic filler. In Fig. 3, the C1s spectra binding energy regions show a very extensive peak, which after deconvolution, is attributed to C–O & C–S, C–C, and C–H, and C–F_3 at 285.51, 284.6, and 291.05 eV (Fig. 3b) [39,40]. The oxygen 1S spectra were large and asymmetric, signaling the presence of more than one chemical state of O in the CPE (Fig. 3c). After curve-fitting, three chemical states of surface O atoms were revealed: O–C at 531.75 eV, O═S at 530.94, and O-M at 530.06 eV, respectively [40,41]. The Li 1s spectra contain the contributions from the Li–N bond for LiTFSI salt and Li–O bond for LSTP ceramic filler at 54.62 and 49.89 eV (Fig. 3d) [42]. The S 2p peak consists of one singlet, which was observed at 167.1 eV for corresponding to the LiTFSI salt structure (Fig. 3e) [43]. F1s peak shows one peak at 686.93 eV for representing the CF_3 bond (Fig. 3f) [42]. For Si 2p spectra, only one chemical structure corresponding to the Si–O bond is observed at a binding energy of 100.23 eV, like the previously reported work (Fig. S3a) [44]. As can be observed in Fig. S3b, the high-resolution Ti $2p_{3/2}$ peak showed clear two distinct peaks at 464.26 and 459.67 eV, which can be indicated to be Ti^{4+}, whereas there is no peak belonging to Ti^{3+}[45]. Fig. S3c shows P 2p signals at 131.23 eV, respectively, indicating the presence of PO_4^{3-} at the surface of the CPEs [46]. There is no big difference between the μm and nm-sized particle-filled in CPE films, and all these XPS spectra above

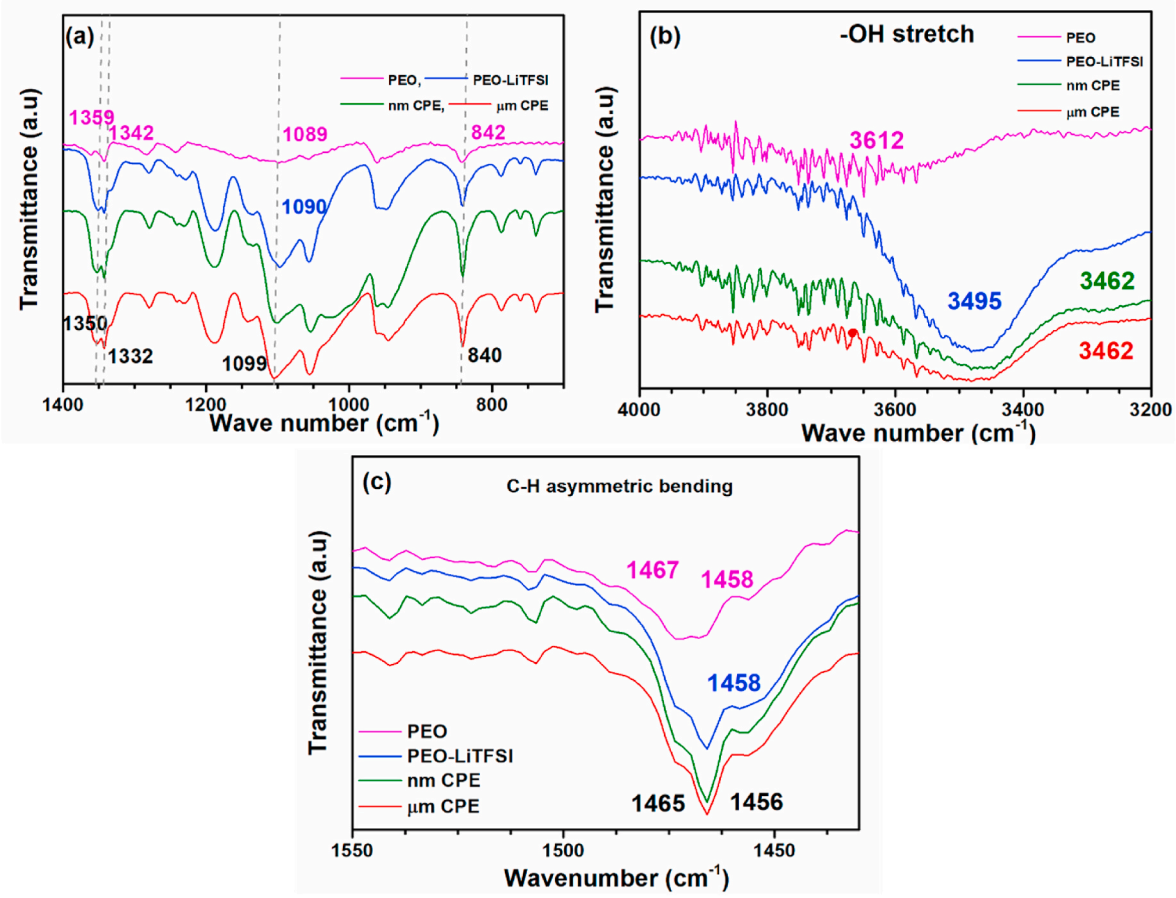

Fig. 2. FTIR spectra of the PEO-based CPE filled with micron and nanosized particulates. (a) PEO-LiTFSI electrolyte *vs.* μm and nm particle-based PEO-LSTP composite polymer electrolyte, (b) –OH stretch, and (c) C–H asymmetric bending.

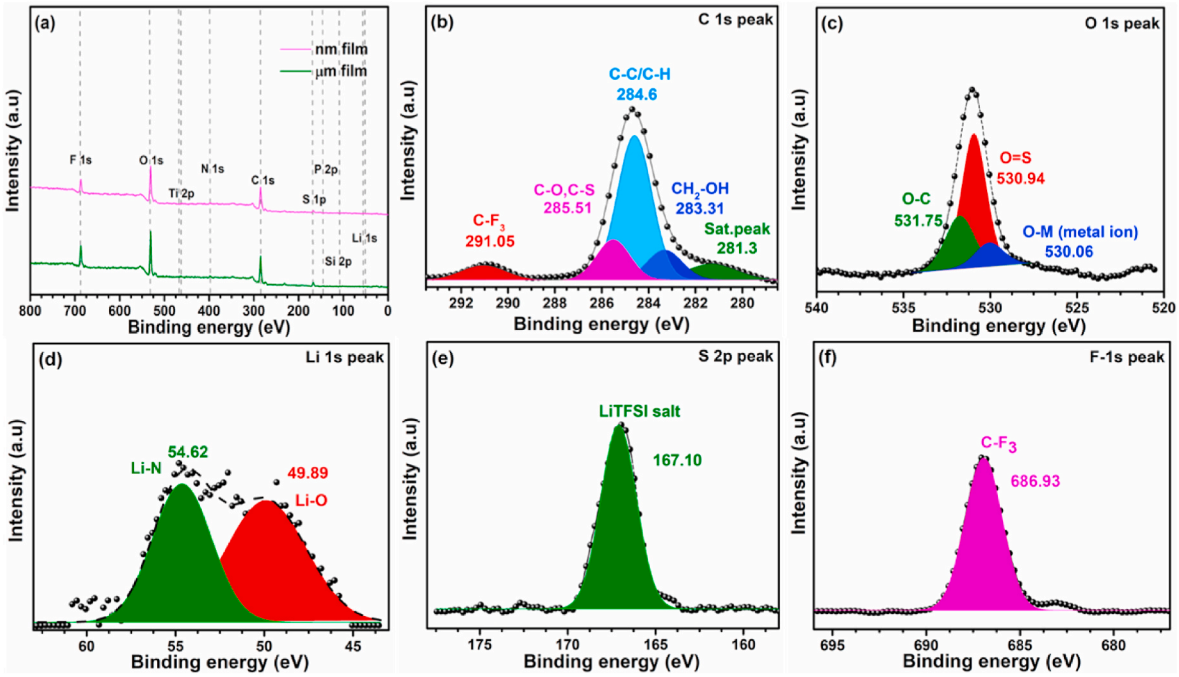

Fig. 3. XPS spectra of the composite polymer electrolyte. (a) Comparison of the full range spectra for the μm and nm particle-based PEO-LSTP composite polymer electrolyte. Deconvoluted spectra of nm-CPE (b) carbon-1s, (c) oxygen-1s, (d) Lithium-1s, (e) sulfur-2p and (f) fluorine -1s elements.

fully support the successful preparation of the CPEs.

Nuclear magnetic resonance (NMR) is an important spectroscopic method to determine the structure of composite polymer electrolytes. Different nuclei may be studied by using the NMR technique, but ^{1}H, ^{13}C, and ^{19}F are the most generally focused elements. The combination of FTIR and NMR data was often enough to determine the complete structure of an electrolyte. Fig. 4 and Fig. S5 show the NMR spectra for the composite polymer electrolyte with micro and nano-sized ceramic filler. A tall singlet resonance at 3.59 ppm corresponds to the characteristic ethylene (–CH_2–CH_2-), whereas the resonance near 2.51 ppm represents the –OH group (Fig. 4a) [47]. In long chains, all the –CH_2 absorptions may be overlapped in an unresolvable group. The multiplets (near at 1.39 ppm) from different carbons generally overlap because the ^{13}C–H coupling constants are frequently larger than the chemical shift differences of the carbons in the spectrum (Fig. 4b) [47]. Quaternary carbon resonance near 70.88 ppm represents the CF_3 in the LiTFSI salt.

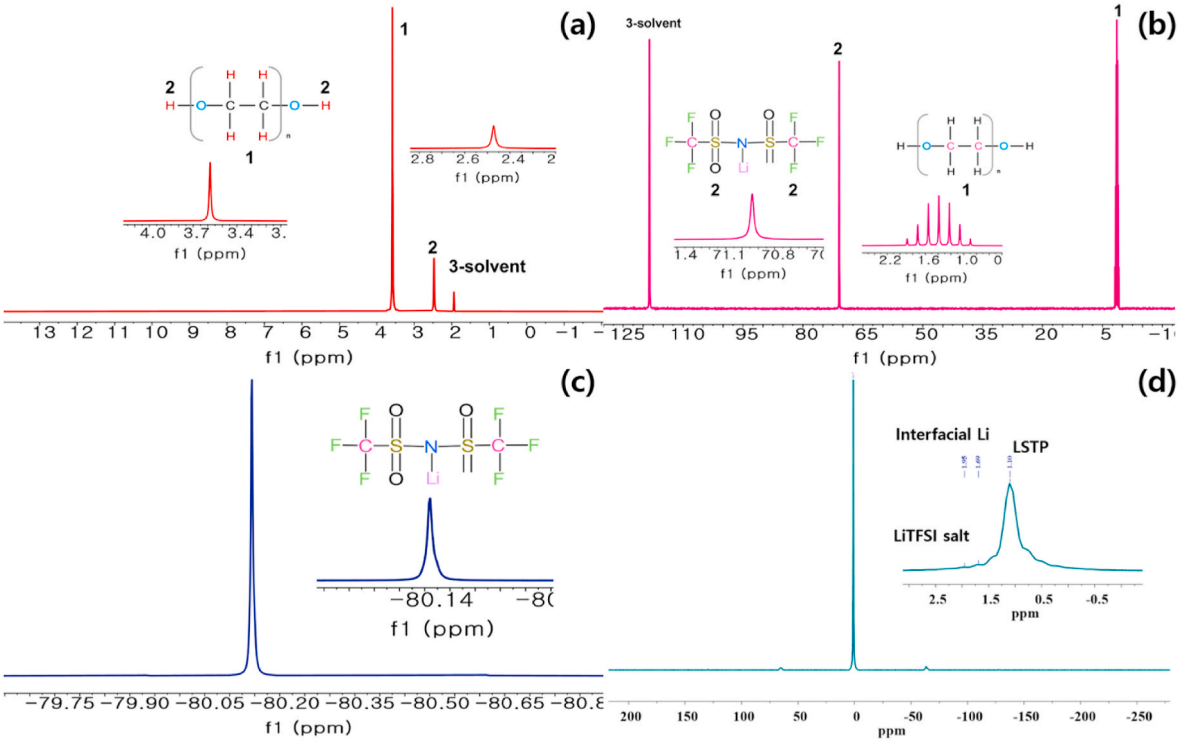

Fig. 4. NMR spectra of the nm-sized composite polymer electrolyte. (a) proton ^{1}H, (b) carbon ^{13}C, (c) fluorine ^{19}F and (d) lithium ^{7}Li.

^{19}F NMR was important to verify whether TFSI- ion presence in the electrolyte plays a major role in the ionic conductivity. From Fig. 4c, we observe a tiny singlet at −80.14 ppm which was assigned to a CF_3 bond with a similar signal observed by previous reports [47,48]. Both the μm and nm CPEs look similar to each other, and there is no difference in their NMR spectra. Fig. 4d shows the MAS solid-state ^{7}Li NMR spectra for the PEO-LiTFSI-LSTP electrolyte. The resonance at 1.69 ppm was assigned to interfacial Li, whereas the resonance at 1.10 and 1.95 ppm corresponded to the Li-ion in LSTP ceramic filler and LiTFSI salt. The interactions confirmed the alternative path at the interface for Li-ion transfer by Li–O segmental motion [49]. The NMR tool confirms the presence of the PEO and LiTFSI salt in the CPE.

3.1.2. Surface morphology of the composite electrolyte

The FE-SEM and TEM were utilized to study the PEO-LSTP-based CPEs with different LSTP-sized particles. Fig. 5a–h and Fig. S6 confirm the morphology of the particles was coarser with irregular shapes, and the average diameter of the micro and nanoparticles were estimated as ~1.07 μm and 430 nm. Fig. 5i and j shows the lower magnification images of the micron and nano-sized CPE. It reveals that both micro and nano-ceramic fillers were well distributed in the PEO matrix with less particle aggregation. Moreover, the CPEs filled with nanosized LSTP had a higher surface area, which could enrich the effective surface area for efficient Lewis acid-base interactions [15]. Overall, the incorporation of the nanoparticles improved the ionic conductivity of the CPE than in the case of the micron-sized filler CPE as shown in the following sections. Fig. 5k and l shows the optical microscopic images of the micro-and nanofiller distribution on the PEO-based CPEs at ambient temperature. Both the CPEs exhibited good macroscopic homogeneity and quasi-uniform morphology, but the difference was its particle/polymer interface region [50,51]. In Fig. 5m and n, the TEM images confirmed the high surface area of the nano-sized filler particles increased the large particle/polymer interface [10,52]. Atomic force microscopy is a useful method for studying the particle size distribution of CPEs. AFM images acquired in this study confirmed that the LSTP particles were uniformly distributed on the PEO-based CPEs. Fig. 5e and f shows slight aggregation in the micron-sized and nano-sized filler-based CPE in the polymer matrix, whereas the ceramic filler is almost completely embedded in the host matrix. The red-colored region on the AFM images represents the LSTP particles. This suggested a strong interaction between the ceramic filler, Li salt, and PEO polymer, which is essential for achieving good ionic conductivity [53]. In addition, the even distribution of the fillers in the host was also expected to result in good electrochemical stability.

3.1.3. Thermal analysis of the composite solid electrolyte

TGA and DSC studies were performed to analyze the thermal stability of the CPEs and alteration of the glass-transition temperature due to the inclusion of the micro-and nanosized LSTP particles. The thermal degradation behavior of the PEO-based CPEs was tested by TGA at a heating rate of 5 °C min^{-1} from 25 to 700 °C. Fig. S7a shows the comparison of the TGA of the 1 μm and 300 nm filled PEO-based CPE. The decomposition of the PEO started at approximately 200 °C, and ~90% weight loss was noted for pure PEO before reaching 400 °C. After incorporation of the micron-sized particles, the onset temperature was shifted to ~250 °C, whereas this was observed at ~290 °C in nanosized filler incorporated CPE. The first weight loss observed was attributed to the thermal degradation of the PEO by the shielding phenomenon [54,55]. Meanwhile, the extended degradation was because of the

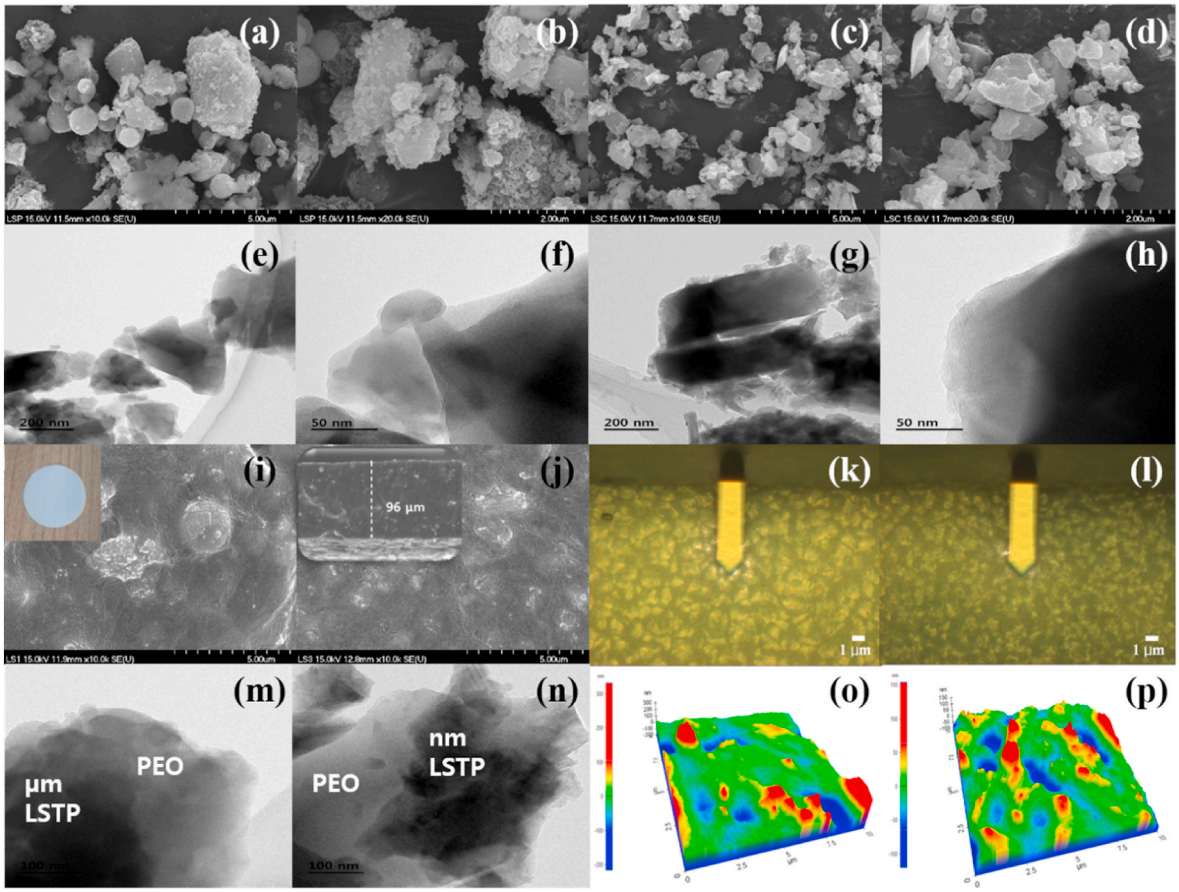

Fig. 5. FE-SEM and TEM images of the LSTP ceramic filler (a–b), (e–f) μm, and (c–d), (g–h) nano-sized particles. FE-SEM, optical microscopic, TEM, and AFM images of the micron and nanosized LSTP particles loaded in the CPEs. (i, k, m, and o) μm size LSTP-filled CPE, and (j, l, n, and p) nm-sized LSTP-filled CPE. Inset images 5i and j. Photographic image of the electrolyte and thickness of the CPE.

exfoliation and intercalation of the complex polymer chains in the presence of the LSTP particles. The interaction between the polymer and ceramic filler induces a strong barrier effect that prevents the thermal decomposition of the complex matrix [54,56]. However, in this study, the strong interaction between the LSTP particle and PEO may have slowed down the exfoliation of the polymer decomposition. After 400 °C, the second weight loss was observed, which was because of the decomposition of the LiTFSI salt [57]. Therefore, the remaining residual samples represented the LSTP phase and showed its stability at a higher temperature.

Fig. S7b shows the DSC thermograms of the PEO-based CPEs as a function of the particle size. The endothermic event observed at ~72 °C corresponded to the melting point of the crystalline PEO polymer [54]. Apparently, the melting temperature of the CPEs decreased with the addition of the Li salt, micro-and nanosized LSTP particles. The μm filler–based CPE melting temperature was 54.3 °C, but in the nm filler–based CPE was further decreased to 51.76 °C. This implies that the particle size enlarges the contact area and decreases the crystal form of the PEO complex. Meanwhile, the low glass-transition temperature indicated the existence of a large number of amorphous phases, which is beneficial for improving Li-ion migration [58].

3.2. Electrochemical performance of the symmetric cell (Li/PEO-LSTP/Li)

3.2.1. Li-ion transference number of the CPEs

The following equation was used to calculate the Li^+-ion transference number (t_{Li+}) of the CPE [59,60].

$$t_{Li+} = \frac{i_s\,(\Delta V - i_o R o')}{i_o\,(\Delta V - i_s R s')}$$

In the above equation, the initial and steady-state currents are represented i_o and i_s, respectively, while V is the polarization voltage, R_o and R_s are the sums of the charge-transfer resistance R_{ct}, and R_{film} is the passivation film resistance. The AC impedance spectra were used to calculate the R_s and R_o of the cell in the frequency range of 1 MHz–10 mHz. The Li/CPE/Li symmetric cell was used to measure the polarization using a DC voltage (ΔV) of 10 mV at 60 °C to achieve a steady state. Table 1 lists the relevant data obtained from the electrochemical studies of the CPEs in non-blocking Li symmetric cells. The combination of the PEO and nanoparticles showed a conspicuous drop in the interfacial resistance, which was beneficial for promoting faster ion transport (Fig. S8a–d). The Li-ion transference numbers for nano- and micron-sized particle filed CPE was found to be 0.45 and 0.36 at 60 °C, respectively (Table 1). The incorporation of nanosized ceramic fillers is beneficial due to the high surface area and larger particle-polymer interface region in the PEO matrix [10,50,61].

3.2.2. Comparative electrochemical impedance spectroscopy and electrochemical stability window (linear sweep voltammetry) of the CPEs

Electrochemical impedance spectroscopy (EIS) was performed to analyze the ionic conductivity of the LSTP pellet and CPE under various temperature conditions, as shown in Fig. S9a and Fig. 6. The ionic conductivity of the LSTP pellet is 1.75×10^{-5} S cm^{-1} at 60 °C and 3.67×10^{-4} S cm^{-1} at 80 °C, and the cell details are shown in supporting information. Fig. 6a and b shows the Nyquist plot of the CPEs in the symmetric cell (SS/CPE/SS) configuration, and the resistance values tend to decrease with increasing temperature. The 25 wt% nm size LSTP particle-filled PEO-based CPE had high ionic conductivity values of 5.44×10^{-4} S cm^{-1} at 60 °C and 1.09×10^{-3} S cm^{-1} at 80 °C, while those of the μm sized particle-filled sample was 4.57×10^{-5} S cm^{-1} and 1.39×10^{-4} S cm^{-1} under similar testing conditions. For comparison, we are testing the ionic conductivity of different wt.% LSTP-based CPEs, and the results are shown in supporting information (Fig. S10). The ionic conductivity improvement is mainly attributed to the strong interactions between the Li-salt, LSTP nanoparticles, and polymer chains, and it is consistently distributed inside the PEO matrix, which eventually prevents recrystallization [15]. Consequently, the amorphous nature of the polymer matrix increased, resulting in better ionic conductivity. Furthermore, the nanoparticle-loaded CPE had low activation energy (0.28 eV) than that of the micron-sized particle-filled CPE (0.50 eV), indicating the effective surface area interactions between the LSTP and polymer chains (Fig. 6C). This suggests that the nanosized LSTP ceramic filler increases the larger particle/polymer interface in the CPEs [10,50,58].

Table 1
Measured values of the initial and steady-state current, impedance, and transference number of the PEO-based CPE filled with 1.07 μm and 430 nm particle sizes of the LSTP electrolytes at 60 °C.

Sample	i_o (μA)	i_s (μA)	R_o/Ω	R_s/Ω	t_{Li+}
μm CPE	35.34	27.61	283.15	284.14	0.36
nm CPE	42.88	35.63	195.71	197.37	0.45

To achieve high energy density ASSLMB, a high-voltage cathode must be used. Thus, a wide electrochemical stability window is essential for CPEs. Linear sweep voltammetry (LSV) was performed to examine the electrochemical stability of the CPEs using a Li/CPE/SS cell with potential in the range of 3–7 V *vs.* Li, as illustrated in Fig. S11. From the LSV curve, both the prepared CPEs were stable up to 5.5 V *vs.* Li because of the incorporation of the LSTP ceramic particles [15]. The CPE showed excellent electrochemical stability in the range of 3–5.2 V *vs.* Li, irrespective of the filler size. This range covers most of the cathode range available in the market for building next-generation high-energy ASSLIBs.

3.2.3. Galvanostatic charge/discharge curve of the symmetric cell

Fig. S9b GCD curve confirms the Li stable nature of the LSTP pellet against Li-metal foil and the Li symmetric cell work up to 100 h. The Li/PEO-LiTFSI-LSTP/Li symmetric cell was used to understand the Li-ion conduction mechanism in the CPE, as shown in Fig. 6d. The current density of the cell of 0.1 mA cm^{-2} was applied every 30 min, while the direction of the current was changed during the charge (Li-plating) and discharge (Li-stripping) processes (Fig. 6d). During the electrochemical cycling, the Li-ions from one electrode moved across the CPE to the other electrode. In the micro filler-based cell, the Li-plating and stripping induced a large overpotential even at a low current density of 0.1 mA cm^{-2}. Meanwhile, the nano-ceramic filler-based cell exhibited excellent electrochemical behavior with low polarization and no indication of dendrite formation at low current densities. These results demonstrate that the nanofiller played a dual role in enhancing the Li-ion conductivity and the electrochemical stability. Therefore, we conclude that the nanofiller-based CPE could be used as a separator-cum-electrolyte for the fabrication of high-energy Li-ion power packs. To understand the uniform Li deposition, we tested the surface morphological analysis of the cycled μm, and nm-sized LSTP particles loaded CPEs. Fig. S12 shows the FE-SEM image of the cycled μm and nm-sized LSTP particles loaded in the CPE. Fig. S12 a–d shows the surface morphology of the CPE after lithium was deposited on the surface at a current density of 0.1 mA cm^{-2} for 20 h. After the lithium deposition, the brownish-black colored layer regions were observed. It indicates that the lithium was uniformly deposited on the surface of the (μm and nm LSTP particle-loaded) CPEs. Additionally, we verified the Li-plating and stripping process of the cell at 0.2 mA cm^{-2} current density (Fig. S13). The initial overpotential of the nano filler-based cell was 0.126 V, but after 100 cycles, it decreased to 0.079 V. Compared to this, the micro filler-based cell overpotential was high due to the particle/polymer interface in the CPE.

3.2.4. Electrochemical performance of the $LiFePO_4$ nm-LSTP CPE/Li cell

As discussed above, the PEO-based nano-LSTP-loaded CPE shows excellent stability and electrochemical performance, enabling it to be used in ASSLMB. The prepared ASSLIB was tested at 60 °C. Fig. 7a shows

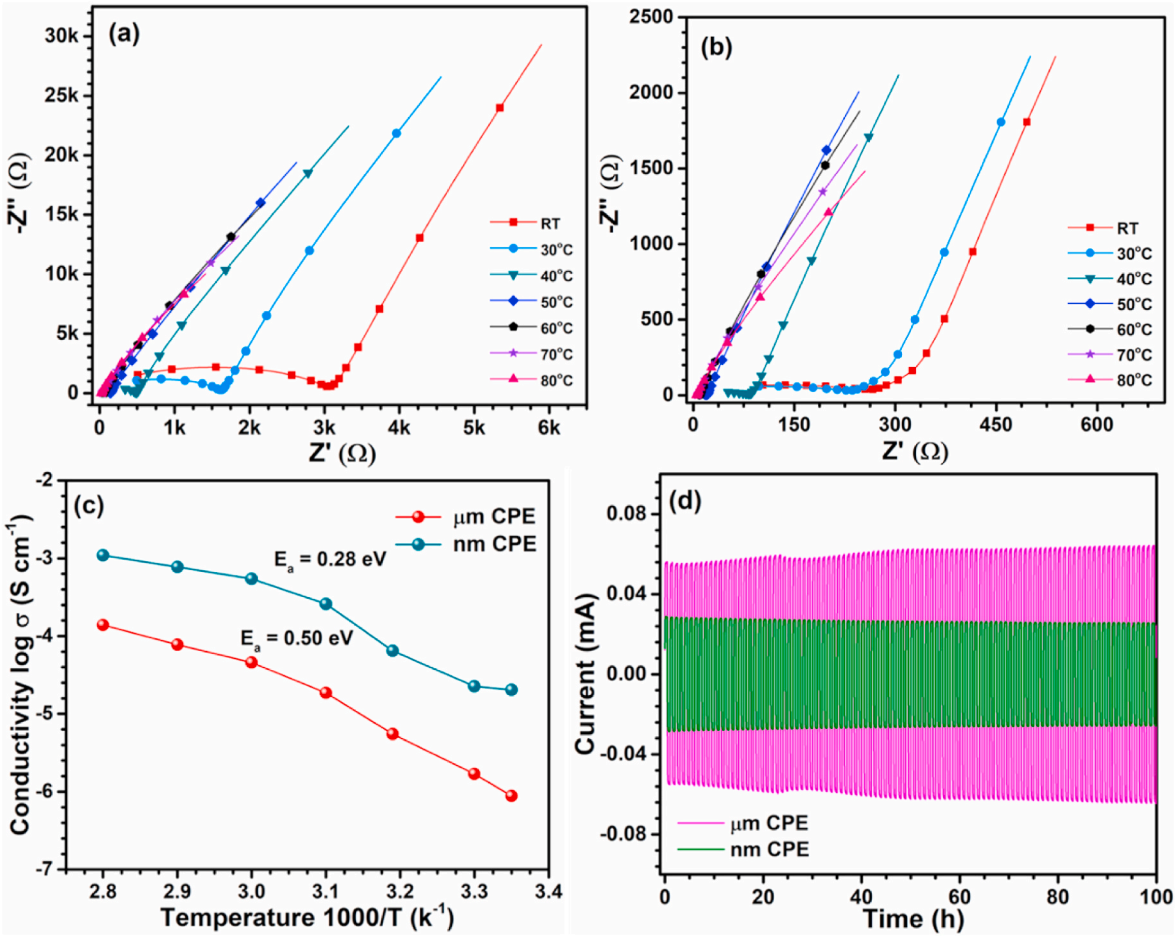

Fig. 6. EIS curve of the symmetric cell for the CPE filled with (a) μm and (b) nm-sized LSTP particles, (c) Arrhenius plot, and (d) Comparison of the galvanostatic charge-discharge curve of the symmetric cell of the μm and nm-sized LSTP particles loaded in the CPE at a current density of 0.1 mA cm^{-2} and the electrochemical performance of the cell was tested at 60 °C.

the profiles of cyclic voltammetry for the $LiFePO_4$/nm-LSTP CPE/Li cell in the potential range of 2.5–4 V at the scan rate of 0.1 mV s^{-1}.

The reaction mechanism of $LiFePO_4$ as follows:

In charging and discharging process:

$$LiFePO_4 \rightleftharpoons xFePO_4 + (1 - x)\ LiFePO_4 + xLi + xe^-$$

From the above reaction mechanism, it can be concluded that the charge-discharge process is carried through a two-phase reaction between $LiFePO_4$ and $FePO_4$. During the charging process, Li-ion de-intercalates from $LiFePO_4$ and forms the $FePO_4$ phase. Again, in the discharging process, the Li-ion intercalates to $FePO_4$ and forms the olivine $LiFePO_4$ phase [62]. A couple of oxidation and reduction peaks at around 3.64 and 3.25 V for the first cycle indicate the charge/discharge process of the cell. No additional cathodic and anodic peaks were observed rather than characteristic peaks that indicate the $LiFePO_4$ has a stable olivine structure in the charging and discharging process and has good electrochemical stability [62,63]. After the first cycle, the oxidation and reduction peak shift to 3.62 and 3.24 V, and there is no difference until the fifth cycle. These studies also confirmed that CPE acted as an ionic conductor in such a potential range.

The plot of the differential capacity (dQ/dV) *vs.* voltage at the 1st, 20th, 50th, and 100th cycles is shown in Fig. 7b. It explains the details of the charge/discharge process. The first cycle displays cathodic and anodic peaks centered at 3.59 and 3.39 V, corresponding to the two-phase charge/discharge reaction of the Fe^{2+}/Fe^{3+} redox couple. After a few cycles, the redox couple shifted to 3.56 and 3.40 V, and the potential difference of the peaks ΔE ~0.14 V reflects the polarization of the ASSLMB. To evaluate the merit of the cathode in the SSBs, galvanostatic characterizations were carried out to examine the specific capacity of the LFP/nm-LSTP CPE/Li cell. In Fig. 7c, we observed the cycling performance of the cell using 1 C-rate charging and discharging. The initial charge and discharge capacities are 129/124 mAh g^{-1}, and the coulombic efficiency of the cell was 96%. For comparison, the prepared LFP/μm-LSTP CPE/Li cell provided the charge/discharge capacities are 106/101 mAh g^{-1}, and the low discharge capacity is due to the low ionic conductivity and smaller particle-polymer interfacial contact between the PEO and μm-LSTP particles (Table S2, Fig. S14). It has been observed that the initial charge capacity is usually much higher than the discharge capacity. This phenomenon is likely a result of the SEI formation in the liquid cell battery [64]. The discharge capacity, capacity retention, and fade rate are summarized in Table 2. After 5 cycles, the discharge capacity is increased to 127 mAh g^{-1} due to the activation process. The cell retains 89% of its initial capacity after 100 cycles, and the capacity fade rate is estimated to be 0.179 mAh g^{-1} per cycle. This stable and excellent cycling performance might be correlated with the high ionic conductivity and improved the interfacial properties of the CPE and inherent mechanical properties of the nano-LSTP. These electrochemical studies revealed that our CPEs exhibited excellent electrochemical performance at 60 °C, comparable with that of LFP-based cathode materials reported previously (Table 3) [8,52,65–68]. But after 200 cycles, the discharge capacity was further decreased to 81 mAh g^{-1}, which corresponds to nearly 66% of its initial discharge capacity (Fig. 7d). A conventional LIB with a liquid electrolyte was also studied (Fig. S15) for comparison.

The reasons for the capacity decay were due to slight volume

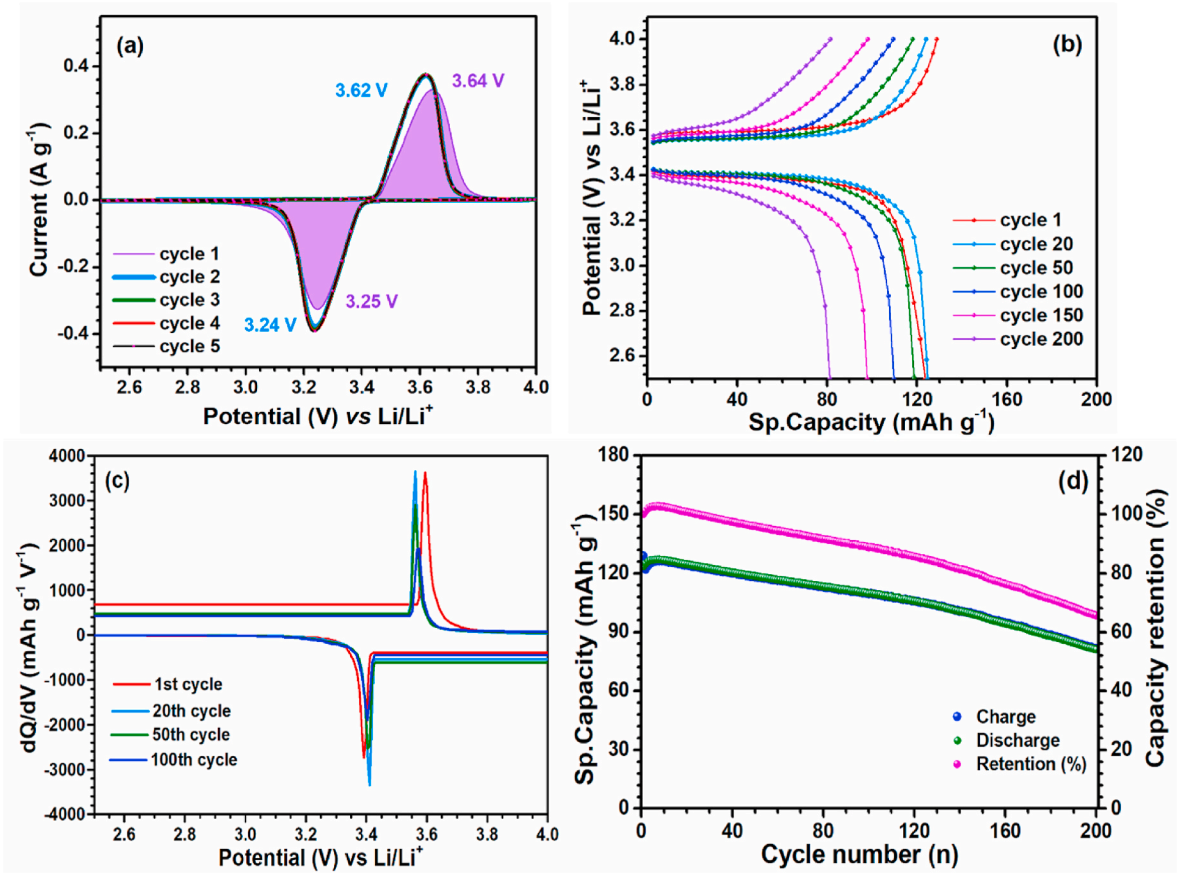

Fig. 7. (a) Cyclic voltammetry for the first 5 cycles under 0.1 mV S^{-1} scan rate, (b) Galvanostatic charge-discharge performance at a rate of 1C for the 1st, 20th, 50th, 100th, and 200th cycles, (c) dQ/dV curve for the 1st, 20th, 50th, and 100th cycle at a rate of 1C and (d) cycle life *vs.* charge/discharge capacity *vs.* capacity retention curve of the $LiFePO_4$/nm-LSTP CPE/Li cell. All the electrochemical tests of the cell were tested at 60 °C.

Table: 2
Capacity retention and capacity fade rate of the Li/nm-LSTP CPE/LFP cell at the 1C rate.

Cycle	Capacity (mAh g^{-1})	Capacity retention (%)	Capacity fade rate (%)
5	127		
50	119	96	0.177
100	110	89	0.179
200	81	66	0.236

expansion, Li-ion irreversibility, Li-ion depletion layer formation, and the slight increment in the charge transfer resistance between the electrode/electrolyte for the long cycle life. Fig. S16 shows the FE-SEM images of the $LiFePO_4$ particles before and after the electrochemical performance. After 200 cycles, the small cracks formed on the LFP particle due to the volume expansion of the electrode. The small cracks limit the Li-ion intercalation in the cathode particle and further decrease the capacity of the cell. Fig. S17 displays the XPS spectra for the $LiFePO_4$ cathode before and after the electrochemical test. After the cycling test, the Li 1s and Fe 2p peaks were slightly shifted, and their intensity was decreased due to Li-ion reduction on the surface. The lithium-ion irreversibility and slight volume expansion lead to the capacity loss of the cell.

Fig. 8a and b shows the initial charge/discharge capacity curves and rate capability curves of a Li/nm-LSTP CPE/$LiFePO_4$ cell at different C rates. The first discharge capacities at rates of 0.1, 0.2, 0.5, 1, and 2C are 160, 151, 139, 128, and 113 mAh g^{-1}, respectively. At high C-rates, the capacity is decreased due to the high polarization of the cell, the charge plateau increases, and the discharging plateau decreases upon increasing the current density. When the current density is switched back to a 0.1C rate, the discharge capacity is almost reached its initial capacity, indicating stable mechanical compatibility and interfacial stability between the cathode and electrolyte. EIS measurements were performed to evaluate the Li/nm-LSTP CPE/LFP cell. Fig. 8c reveals AC impedance spectra of the ASSLMB before and after 200 cycles at 1C at 60 °C. As shown by the results, the charge-transfer resistance of the cell

Table:3
The electrochemical performance of Li metal batteries using a different kinds of solid electrolytes using PEO polymer matrix.

Solid electrolyte	Ionic conductivity	Cathode	Electrochemical performance	Ref.
PEO/LiTFSI + LAGP	6.76×10^{-4} S cm^{-1} at 60 °C	$LiFePO_4$	143 mAh g^{-1} under 0.5C at 60 °C	[8]
PEO/LiTFSI + LLZO particles	2.1×10^{-4} S cm^{-1} at 30 °C	$LiFe_{0.15}Mn_{0.85}PO_4$	107 mAh g^{-1} after 200 cycles under 0.1C at 60 °C	[52]
PEO/LiTFSI+10 wt% LLZTO particles	1.17×10^{-4} S cm^{-1} at 30 °C	$LiFePO_4$	127 mAh g^{-1} after 200 cycles under 0.2C at 55 °C	[65]
PEO/LiTFSI + LATP/PAN nanofiber	6.5×10^{-4} S cm^{-1} at 60 °C	$LiFePO_4$	144 mAh g^{-1} after 100 cycles under 0.2C at 60 °C	[66]
PEO/LiTFSI-LLZTO	6.57×10^{-4} S cm^{-1} at 80 °C	$LiFePO_4$	125.5 mAh g^{-1} under 1C at 80 °C	[67]
PEO/LiClO4 + LLZO	1.93×10^{-3} S cm^{-1} at 70 °C	$LiFePO_4$	135.98 mAh g^{-1} under 0.2C at 70 °C	[68]
PEO/LiTFSI + nm-LSTP	1.09×10^{-3} S cm^{-1} at 80 °C	$LiFePO_4$	110 mAh g^{-1} after 100 cycles under 1C at 60 °C	This work

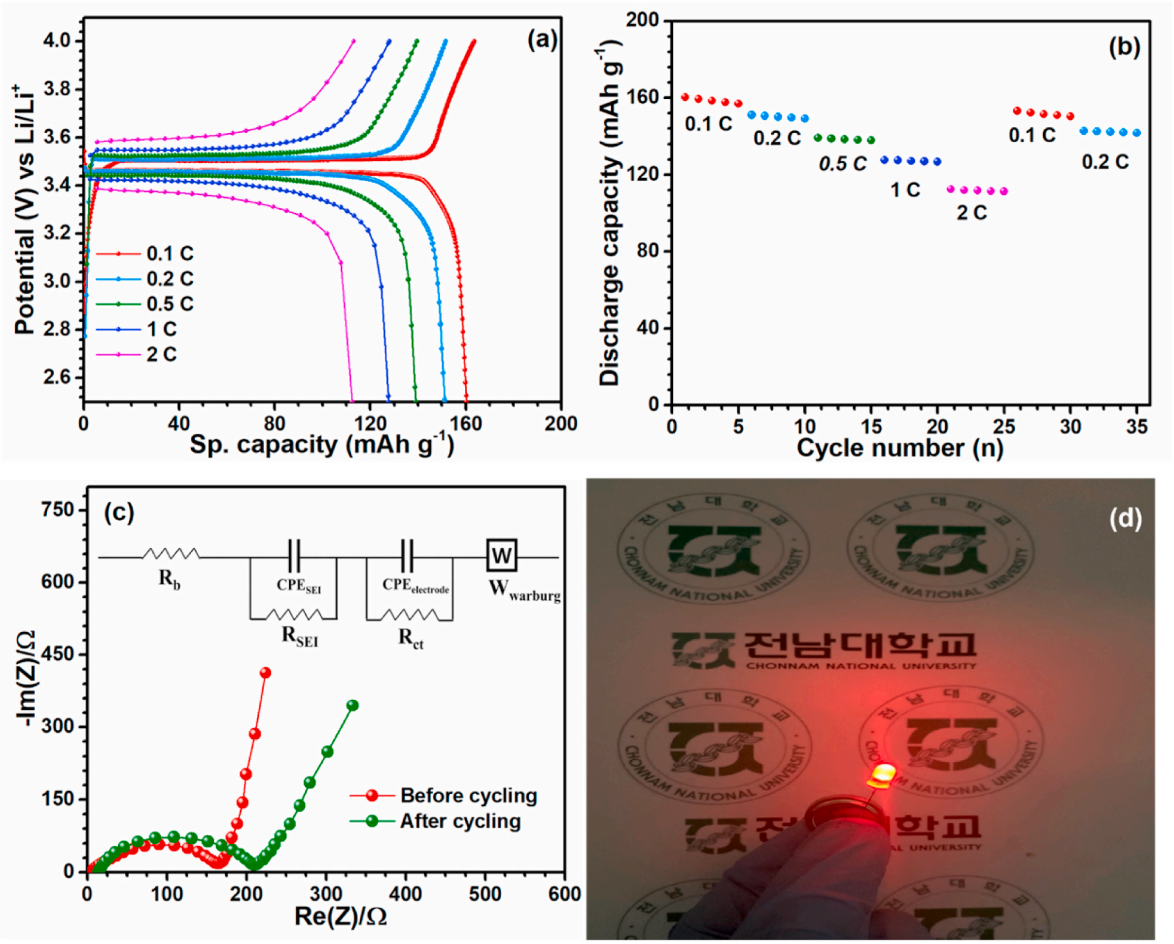

Fig. 8. (a) Rate capability curve, (b) cycle life of the cell tested under different C-rate, (c) Electrochemical impedance spectra study of the cell before and after 200 cycles test. The electrochemical performances were studied at 60 °C.

increased from 113 to 142 Ω after the 200-cycle test. The small increment in the charge transfer resistance indicated good interfacial compatibility and superior interfacial stability with an electrode which was attributed to the flexibility and electrochemical stability of the electrolyte. Furthermore, the coin-cell (ASSLMB) can power a red LED light continuously (Fig. 8d). This test fully proves the reliability of our Li-ion SSB in real-time applications. This study reveals that the nano-sized LSTP-filled PEO-based CPE could be used as a potential electrolyte in the fabrication of ASSLMB.

4. Conclusion

We explored the PEO-based CPE with different sizes (1.07 μm and 430 nm) of the ceramic filler to ascertain particle/polymer interface using a combination of diagnostics techniques, such as FE-SEM, TEM, optical microscopy, and AFM. We observed that the nano-LSTP-loaded PEO-based CPE exhibited a high Li-ionic conductivity of 5.44×10^{-4} S cm^{-1} with a transference number of 0.45 at 60 °C compared to other micron-sized fillers. Furthermore, we showed that the electrochemical stability of the CPEs could be successfully enhanced at higher current densities (0.1 mA cm^{-2}) during Li-plating and stripping studies. Enhanced electrochemical stability was achieved by hosting nanosized LSTP fillers in the polymer matrix. The assembled $LiFePO_4$ nm-LSTP CPE/Li composite solid-state battery had a high capacity of 110 mAh g^{-1} (after 100 cycles under 1C at 60 °C) with a characteristic two-phase reaction and stable cycling profile. Considering the particle size and surface area of the LSTP, its interaction with the polymer backbone enables progress toward the fabrication of high-energy next-generation advanced Li-metal batteries.

Credit author statement

Balasubramaniam Ramkumar: Conceptualization, Methodology, Validation, Formal analysis, Data Curation, Writing Original draft, Visualization, Software. **Vanchiappan Aravindan**: Writing –Review & Editing, Supervision, Funding acquisition, Project administration. **Ramasamy Hari Vignesh**: Writing-Review & Edition. **Kanalli V. Ajeya :** Software. **Ryu Je-gwang**: Data Curation. **Jung Ho-Young:** Software. **Yun-Sung Lee**: Supervision, Resources, Funding acquisition, Project administration.

Declaration of competing interest

The authors declare that they have no known competing financial interests or personal relationships that could have appeared to influence the work reported in this paper.

Acknowledgments

The author would like to thank Jeong Kwan. Co. Ltd for their consistent support. This work was supported by the National Research Foundation of Korea Grant funded by the Korean government (Ministry of Science, ICT and Future Planning) No. 2019R1A2C1007620. VA acknowledges financial support from the Science and Engineering Research Board, a statutory body of the Department of Science and Technology, Govt. of India, through Swarnajayanti Fellowship (SB/SJF/

2020–21/12).

Appendix A. Supplementary data

Supplementary data to this article can be found online at https://doi.org/10.1016/j.solidstatesciences.2022.106958.

References

[1] S. Yuvaraj, S. Amaresh, Y.S. Lee, R.K. Selvan, Effect of carbon coating on the electrochemical properties of Co_2SnO_4 for negative electrodes in Li-ion batteries, RSC Adv. 4 (2014) 6407–6416, https://doi.org/10.1039/c3ra46588h.

[2] S.B. Lee, B. Ramkumar, Double-shelled hybrid MgFe2O4/Fe2O3 hollow microspheres as a high-capacity anode for lithium-ion batteries, J. Ind. Eng. Chem. 110 (2022) 262–273, https://doi.org/10.1016/j.jiec.2022.03.001.

[3] B. Ramkumar, S. Yuvaraj, S. Surendran, K. Pandi, H.V. Ramasamy, Y.S. Lee, R. K. Selvan, Synthesis and characterization of carbon coated LiCo1/3Ni1/3Mn1/3O2 and bio-mass derived graphene like porous carbon electrodes for aqueous Li-ion hybrid supercapacitor, J. Phys. Chem. Solid. 112 (2018) 270–279, https://doi.org/10.1016/j.jpcs.2017.09.012.

[4] J.Y. Hwang, S.J. Park, C.S. Yoon, Y.K. Sun, Customizing a Li-metal battery that survives practical operation conditions for electric vehicle applications, Energy Enviro. Sci. 12 (2019) 2174–2184, https://doi.org/10.1039/c9ee00716d.

[5] H.V. Ramasamy, S. Sinha, J. Park, M. Gong, V. Aravindan, J. heo and Y.S. Lee, Enhancement of electrochemical activity of ni-rich $LiNi_{0.8}Mn_{0.1}Co_{0.1}O_2$ by precisely controlled Al_2O_3 nanocoatings via atomic layer deposition, J. Electrochem. Sci. Technol. 10 (2019) 196–205, https://doi.org/10.5229/JECST.2019.10.2.196.

[6] J. Zagórski, J.M. López Del Amo, M.J. Cordill, F. Aguesse, L. Buannic, A. Llordés, Garnet-polymer composite electrolytes: new insights on local Li-ion dynamics and electrodeposition stability with Li metal anodes, ACS Appl. Energy Mater. 2 (2019) 1734–1746, https://doi.org/10.1021/acsaem.8b01850.

[7] X.B. Cheng, T.Z. Hou, R. Zhang, H.J. Peng, C.Z. Zhao, J.Q. Huang, Q. Zhang, Dendrite-free lithium deposition induced by uniformly distributed lithium ions for efficient lithium metal batteries, Adv. Mater. 28 (2016) 2888–2895, https://doi.org/10.1002/adma.201506124.

[8] Y. Zhao, Z. Huang, S. Chen, B. Chen, J. Yang, Q. Zhang, F. Ding, Y. Chen, X. Xu, A promising PEO/LAGP hybrid electrolyte prepared by a simple method for all-solid-state lithium batteries, Solid State Ionics 295 (2016) 65–71, https://doi.org/10.1016/j.ssi.2016.07.013.

[9] L. Zhu, P. Zhu, Q. Fang, M. Jing, X. Shen, L. Yang, A novel solid PEO/LLTO-nanowires polymer composite electrolyte for solid-state lithium-ion battery,, Electrochim. Acta 292 (2018) 718–726, https://doi.org/10.1016/j.electacta.2018.10.005.

[10] Z. Li, H.M. Huang, J.K. Zhu, J.F. Wu, H. Yang, L. Wei, X. Guo, Ionic conduction in composite polymer electrolytes: case of PEO: Ga-LLZO composites, ACS Appl. Mater. Interfaces 11 (2019) 784–791, https://doi.org/10.1021/acsami.8b17279.

[11] X. Ban, W. Zhang, N. Chen, C. Sun, A high-performance and durable poly(ethylene oxide)-based composite solid electrolyte for all solid-state lithium battery, J. Phys. Chem. C 122 (2018) 9852–9858, https://doi.org/10.1021/acs.jpcc.8b02556.

[12] C. Wang, T. Yang, W. Zhang, H. Huang, Y. Gan, Y. Xia, X. He, J. Zhang, Hydrogen bonding enhanced SiO2/PEO composite electrolytes for solid-state lithium batteries, J. Mater. Chem. 10 (2022) 3400–3408, https://doi.org/10.1039/d1ta10607d.

[13] Z. Xue, D. He, X. Xie, Poly(ethylene oxide)-based electrolytes for lithium-ion batteries, J. Mater. Chem. 3 (2015) 19218–19253, https://doi.org/10.1039/c5ta03471j.

[14] P. Yao, H. Yu, Z. Ding, Y. Liu, J. Lu, M. Lavorgna, J. Wu, X. Liu, Review on polymer-based composite electrolytes for lithium batteries, Front. Chem. 7 (2019), 522, https://doi.org/10.3389/fchem.2019.00522.

[15] D. Lin, W. Liu, Y. Liu, H.R. Lee, P.C. Hsu, K. Liu, Y. Cui, High ionic conductivity of composite solid polymer electrolyte via in situ synthesis of monodispersed SiO2 nanospheres in poly(ethylene oxide), Nano Lett. 16 (2016) 459–465, https://doi.org/10.1021/acs.nanolett.5b04117.

[16] G. Piana, F. Bella, F. Geobaldo, G. Meligrana, C. Gerbaldi, PEO/LAGP hybrid solid polymer electrolytes for ambient temperature lithium batteries by solvent-free, "one pot" preparation, J. Energy Storage 26 (2019), 100947, https://doi.org/10.1016/j.est.2019.100947.

[17] B. Ramkumar, K. So-young, N. Chan-woo, V. Aravindan, L. Yun-Sung, $LiBO_2$-modified $LiCoO_2$ as an efficient cathode with garnet framework $Li_{6.75}La_3Zr_{1.75}Nb_{0.25}O_{12}$ electrolyte toward building all-solid-state lithium battery for high-temperature operation, Electrochim. Acta 359 (2020), 136955, https://doi.org/10.1016/j.electacta.2020.13695518.

[18] B. Ramkumar, C.W. Nam, V. Aravindan, D. Eum, K. Kang, Y.S. Lee, Interfacial engineering in a cathode composite based on garnet-type solid-state Li-ion battery with high voltage cycling, Chemelectrochem 8 (2021) 570–576, https://doi.org/10.1002/celc.202001116.

[19] T.Q. Yang, C. Wang, W.K. Zhang, Y. Xia, Y.P. Gan, H. Huang, X.P. He, J. Zhang, Composite polymer electrolytes reinforced by a three-dimensional polyacrylonitrile/Li0.33La0.557TiO3 nanofiber framework for room-temperature dendrite-free all-solid-state lithium metal battery, Rare Met. 41 (2022) 1870–1879, https://doi.org/10.1007/s12598-021-01891-1.

[20] Y. Jiang, X. Yan, Z. Ma, P. Mei, W. Xiao, Q. You, Y. Zhang, Development of the PEO based solid polymer electrolytes for all-solid state lithium ion batteries, Polymers 10 (2018), 1237, https://doi.org/10.3390/polym10111237.

[21] Y. Sun, X. Zhan, J. Hu, Y. Wang, S. Gao, Y. Shen, Y.T. Cheng, Improving ionic conductivity with bimodal-sized $Li_7La_3Zr_2O_{12}$ fillers for composite polymer electrolytes, ACS Appl. Mater. Interfaces 11 (2019) 12467–12475, https://doi.org/10.1021/acsami.8b21770.

[22] J. Zhang, C. Zheng, J. Lou, Y. Xia, C. Liang, H. Huang, Y. Gan, X. Tao, W. Zhang, Poly(ethylene oxide) reinforced Li6PS5Cl composite solid electrolyte for all-solid-state lithium battery: enhanced electrochemical performance, mechanical property and interfacial stability, J. Power Sources 412 (2019) 78–85, https://doi.org/10.1016/j.jpowsour.2018.11.036.

[23] Y. Liu, Y. Zhao, W. Lu, L. Sun, L. Lin, M. Zheng, X. Sun, H. Xie, PEO based polymer in plastic crystal electrolytes for room temperature high-voltage lithium metal batteries, Nano Energy 88 (2021), 106205, https://doi.org/10.1016/j.nanoen.2021.106205.

[24] X. Wang, Y. Zhang, X. Zhang, T. Liu, Y.H. Lin, L. Li, Y. Shen, C.W. Nan, Lithium-salt-rich PEO/$Li_{0.3}La_{0.557}TiO_3$ interpenetrating composite electrolyte with three-dimensional ceramic nano-backbone for all-solid-state lithium-ion batteries, ACS Appl. Mater. Interfaces 10 (2018) 24791–24798, https://doi.org/10.1021/acsami.8b06658.

[25] J. Lee, T. Howell, M. Rottmayer, J. Boeckl, H. Huang, Free-standing PEO/LiTFSI/LAGP composite electrolyte membranes for applications to flexible solid-state lithium-based batteries, J. Electrochem. Soc. 166 (2019) A416–A422, https://doi.org/10.1149/2.1321902jes.

[26] H.T. Ahmed, O.G. Abdullah, Structural and ionic conductivity characterization of PEO: MC-NH4I proton-conducting polymer blend electrolytes based films, Results Phys. 16 (2020), 102861, https://doi.org/10.1016/j.rinp.2019.102861.

[27] N.M. Jurado-Meneses, M.I. Delgado-Rosero, M.A. Meléndez-Lira, Structural and vibrational studies on composites polymer electrolytes $(PEO)_{10}CF_3COONa$ + x wt. % Al_2O_3, Rev. Fac. Ing. 83 (2017) 43–49, https://doi.org/10.17533/udea.redin.n83a06.

[28] S.B. Aziz, R.B. Marif, M.A. Brza, A.N. Hassan, H.A. Ahmad, Y.A. Faidhalla, M.F. Z. Kadir, Structural, thermal, morphological and optical properties of PEO filled with biosynthesized Ag nanoparticles: new insights to band gap study, Results Phys. 13 (2019), https://doi.org/10.1016/j.rinp.2019.102220. Article.102220.

[29] A.M. Stephan, T.P. Kumar, M.A. Kulandainathan, N.A. Lakshmi, Chitin-incorporated poly (ethylene oxide) -based nanocomposite electrolytes for lithium batteries, J. Phys. Chem. B 113 (2009) 1963–1971, https://doi.org/10.1021/jp808640j.

[30] E.M. Masoud, A.A. El-Bellihi, W.A. Bayoumy, M.A. Mousa, Effect of $LiAlO_2$ nanoparticle filler concentration on the electrical properties of PEO-$LiClO_4$ composite, Mater. Res. Bull. 48 (2013) 1148–1154, https://doi.org/10.1016/j.materresbull.2012.12.012.

[31] A.K. Thakur, S.A. Hashmi, Polymer matrix-filler interaction mechanism for modified ion transport and glass transition temperature in the polymer electrolyte composites, Solid State Ionics 181 (2010) 1270–1278, https://doi.org/10.1016/j.ssi.2010.06.055.

[32] M.F. Shukur, R. Ithnin, H.A. Illias, M.F.Z. Kadir, Proton conducting polymer electrolyte based on plasticized chitosan-PEO blend and application in electrochemical devices, Opt. Mater. (Amst) 35 (2013) 1834–1841, https://doi.org/10.1016/j.optmat.2013.03.004.

[33] M. Echeverri, N. Kim, T. Kyu, Ionic conductivity in relation to ternary phase diagram of poly(ethylene oxide), succinonitrile, and lithium bis(trifluoromethane) sulfonimide blends, Macromolecules 45 (2012) 6068–6077, https://doi.org/10.1021/ma3008509.

[34] H. Wang, H. Zhang, Y. Cheng, K. Feng, X. Li, H. Zhang, Rational design and synthesis of $LiTi_2(PO_4)_3$−xF_x anode materials for high-performance aqueous lithium ion batteries, J. Mater. Chem. 5 (2017) 593–599, https://doi.org/10.1039/c6ta08257b.

[35] G. Wang, X. Wang, L. Yi, L. Wang, R. Yu, M. Liu, D. Wang, Q. Ren, X. Yang, The effects of $LiTi_2(PO_4)_3$ modification on the performance of spherical $Li_{1.5}Ni_{0.25}Mn_{0.75}O_{2+\delta}$ cathode material, RSC Adv. 6 (2016) 46325–46335, https://doi.org/10.1039/c6ra06169a.

[36] S. He, Y. Xu, B. Zhang, X. Sun, Y. Chen, Y. Jin, Unique rhombus-like precursor for synthesis of $Li_{1.3}Al_{0.3}Ti_{1.7}(PO_4)_3$ solid electrolyte with high ionic conductivity, Chem. Eng. J. 345 (2018) 483–491, https://doi.org/10.1016/j.cej.2018.03.151.

[37] E. Zhao, Y. Guo, G. Xu, L. Yuan, J. Liu, X. Li, L. Yang, J. Ma, Y. Li, S. Fan, High ionic conductivity Y doped $Li_{1.3}Al_{0.3}Ti_{1.7}(PO_4)_3$ solid electrolyte, J. Alloys Compd. 782 (2019) 384–391, https://doi.org/10.1016/j.jallcom.2018.12.18.

[38] B. Yang, X. Li, H. Guo, Z. Wang, W. Xiao, Preparation and properties of $Li_{1.3}Al_{0.3}Ti_{1.7}(PO_4)_3$ by spray-drying and post-calcining method, J. Alloys Compd. 643 (2015) 181–185, https://doi.org/10.1016/j.jallcom.2015.04.019.

[39] Z. Geng, J. Lu, Q. Li, J. Qiu, Y. Wang, J. Peng, J. Huang, W. Li, X. Yu, H. Li, Lithium metal batteries capable of stable operation at elevated temperature, Energy Storage Mater. 23 (2019) 646–652, https://doi.org/10.1016/j.ensm.2019.03.005.

[40] R. Blanga, L. Burstein, M. Berman, S.G. Greenbaum, D.J. Golodnitsky, Solid polymer-in-ceramic electrolyte formed by electrophoretic deposition, Electrochem. Soc. 162 (2015) D3084–D3089, https://doi.org/10.1149/2.0221511jes.

[41] W.A. Zoubi, J.H. Min, Y.G. Ko, Hybrid organic-inorganic coatings via electron transfer behaviour, Sci. Rep. 7 (2017), 7063, https://doi.org/10.1038/s41598-017-07691-x.

[42] Z. Zhuang, L. Yang, B. Ju, G. Lei, Q. Zhou, H. Liao, A. Yin, Z. Deng, Y. Rang, S. Qin, F. Tu, Ameliorating interfacial issues of $LiNi_{0.5}Co_{0.2}Mn_{0.3}O_2$/Poly(propylene carbonate) by introducing graphene interlayer for all-solid-state lithium batteries, ChemistrySelect 5 (2020) 2291–2299, https://doi.org/10.1002/slct.201904868.

[43] C. Xu, B. Sun, T. Gustafsson, K. Edström, D. Brandell, M. Hahlin, Interface layer formation in solid polymer electrolyte lithium batteries: an XPS study, J. Mater. Chem. 2 (2014) 7256–7264, https://doi.org/10.1039/c4ta00214h.
[44] S. Li, F. Chen, F. Lin, Y. Kong, H. Dai, Adsorption performance of SiO_2/CPAM composites for aqueous Ca(II), Bioresources 13 (2018) 3554–3570, https://doi.org/10.15376/biores.13.2.3554-3570.
[45] J. Ye, C. Li, Synthesis of $LiTi_2(PO_4)_3$@carbon anode material with superior performance using β-cyclodextrin as carbon sources, Ionics 26 (2020) 2845–2853, https://doi.org/10.1007/s11581-020-03440-9.
[46] A. Kizilaslan, M. Kirkbinar, T. Cetinkaya, H. Akbulut, Sulfur doped $Li_{1.3}Al_{0.3}Ti_{1.7}(PO_4)_3$ solid electrolytes with enhanced ionic conductivity and a reduced activation energy barrier, Phys. Chem. Chem. Phys. 22 (2020) 17221–17228, https://doi.org/10.1039/d0cp03442h.
[47] D.L. Pavia, G.M. Lampman, G.S. Kriz, J.R. Vyvyan, Introduction to spectroscopy, in: Brooks/cole Cemgage Learning, United State of america, fourth ed., 2008.
[48] K.U. Schwenke, J. Herranz, H.A. Gasteiger, M. Piana, Reactivity of the ionic liquid Pyr14TFSI with superoxide radicals generated from KO_2 or by contact of O_2 with $Li_7Ti_5O_{12}$, J. Electrochem. Soc. 162 (2015) A905–A914, https://doi.org/10.1149/2.0241506jes.
[49] M.B. Berman, S.G. Greenbaum, NMR studies of solvent-free ceramic composite polymer electrolytes—a brief review, Membranes (Basel) 5 (2015) 915–923, https://doi.org/10.3390/membranes5040915.
[50] N. Meng, X. Zhu, F. Lian, Particles in composite polymer electrolyte for solid-state lithium batteries: a review, Particuology 60 (2021) 14–36, https://doi.org/10.1016/j.partic.2021.04.002.
[51] H.K. Koduru, Y.G. Marinov, G.B. Hadjichristov, A.G. Petrov, N. Godbert, N. caramuzza, Polyethylene oxide (PEO) – liquid crystal (E8) composite electrolyte membranes: microstructural, electrical conductivity and dielectric studies, J. Non-Cryst. Solids 499 (2018) 107–116, https://doi.org/10.1016/j.jnoncrysol.2018.07.006.
[52] J. Zhang, N. Zhao, M. Zhang, Y. Li, P.K. Chu, X. Guo, Z. Di, X. Wang, H. Li, Flexible and ion-conducting membrane electrolytes for solid-state lithium batteries: dispersion of garnet nanoparticles in insulating polyethylene oxide, Nano Energy 28 (2016) 447–454, https://doi.org/10.1016/j.nanoen.2016.09.002.
[53] P. Prabakaran, R.P. Manimuthu, S. Gurusamy, Influence of barium titanate nanofiller on PEO/PVdF-HFP blend-based polymer electrolyte membrane for Li-battery applications, J. Solid State Electrochem. 21 (2017) 1273–1285, https://doi.org/10.1007/s10008-016-3477-z.
[54] D.I. Iermakova, R. Dugas, M.R. Palacín, A. Ponrouch, On the comparative stability of Li and Na metal anode interfaces in conventional alkyl carbonate electrolytes, J. Electrochem. Soc. 162 (2015) A7060–A7066, https://doi.org/10.1149/2.0091513jes.
[55] N.K. Singh, M.L. Verma, M. Minakshi, PEO nanocomposite polymer electrolyte for solid state symmetric capacitors, Bull. Mater. Sci. 38 (2015) 1577–1588, https://doi.org/10.1007/s12034-015-0980-2.
[56] N. Angulakshmi, K.S. Nahm, J.R. Nair, C. Gerbaldi, R. Bongiovanni, N. Penazzi, A. M. Stephan, Cycling profile of $MgAl_2O_4$-incorporated composite electrolytes composed of PEO and $LiPF_6$ for lithium polymer batteries, Electrochim. Acta 90 (2013) 179–185, https://doi.org/10.1016/j.electacta.2012.12.003.
[57] K. Liu, R. Zhang, J. Sun, M. Wu, T. Zhao, Polyoxyethylene (PEO)|PEO-Perovskite|PEO composite electroyte for all-solid-state lihtium metal batteries, ACS Appl. Mater. Interfaces 11 (2019) 46930–46937, https://doi.org/10.1021/acsami.9b16936.
[58] K.S. Ji, H.S. Moon, J.W. Kim, J.W. Park, Role of functional nano-sized inorganic fillers in poly(ethylene) oxide-based polymer electrolytes, J. Power Sources 117 (2003) 124–130, https://doi.org/10.1016/S0378-7753(03)00159-9.
[59] M. Riley, P.S. Fedkiw, S.A. Khan, Transport properties of lithium hectorite-based composite electrolytes, J. Electrochem. Soc. 149 (2002), A667, https://doi.org/10.1149/1.1470652.
[60] J. Zhao, L. Wang, X. He, C. Wan, C. Jiang, Determination of lithium-ion transference numbers in $LiPF_6$–PC solutions based on electrochemical polarization and NMR measurements, J. Electrochem. Soc. 155 (2008), A292, https://doi.org/10.1149/1.2837832.
[61] I. Chakraborty, K.J. Bodurtha, N.J. Heeder, M.P. Godfrin, A. Tripathi, R.H. Hurt, A. Shukla, A. Bose, Massive electrical conductivity enhancement of multilayer graphene/polystyrene composites using a nonconductive filler, ACS Appl. Mater. Interfaces 6 (2014) 16472–16475, https://doi.org/10.1021/am5044592.
[62] Y.Q. Hu, H.P. Liu, Y. Zhang, K.F. Liu, Charging method research for lithium iron phosphate battery, Procedia Eng. 15 (2011) 4367–4371, https://doi.org/10.1016/j.proeng.2011.08.820.
[63] C. Chen, G.B. Liu, Y. Wang, J.L. Li, H. Liu, Preparation and electrochemical properties of $LiFePO_4$/C nanocomposite using $FePO_4{\cdot}2H_2O$ nanoparticles by introduction of $Fe_3(PO_4)_2{\cdot}8H_2O$ at low cost, Electrochim. Acta 113 (2013) 464–469, https://doi.org/10.1016/j.electacta.2013.09.095.
[64] X. Yu, Y. Liu, J.B. Goodenough, A. Manthiram, Rationally designed PEGDA−LLZTO composite electrolyte for SolidState lithium batteries, ACS Appl. Mater. Interfaces 13 (2021) 30703–30711, https://doi.org/10.1021/acsami.1c07547.
[65] L. Chen, Y. Li, S.P. Li, L.Z. Fan, C.W. Nan, J.B. Goodenough, PEO/garnet composite electrolytes for solid-state lithium batteries: from “ceramic-in-polymer” to “polymer-in-ceramic”, Nano Energy 46 (2018) 176–184, https://doi.org/10.1016/j.nanoen.2017.12.037.
[66] D. Li, L. Chen, T. Wang, L.Z. Fan, 3D fiber-network-reinforced bicontinuous composite solid electrolyte for dendrite-free lithium metal batteries, ACS Appl. Mater. Interfaces 10 (2018) 7069–7078, https://doi.org/10.1021/acsami.7b18123.
[67] F. Zeng, Y. Sun, B. Hui, Y. Xia, Y. Zou, X. Zhang, D. Yang, Three-dimensional porous alginate fiber membrane reinforced PEO-based solid polymer electrolyte for safe and high-performance lithium ion batteries, ACS Appl. Mater. Interfaces 12 (2020) 43805–43812, https://doi.org/10.1021/acsami.0c13039.
[68] K. Heo, J. Im, J.S. Lee, J. Jo, S. Kim, J. Kim, J. Lim, High-rate blended cathode with mixed morphology for all-solid-state li-ion batteries, J Electrochem Sci Technol 11 (2020) 282–290, https://doi.org/10.33961/jecst.2019.00661.